

# High-Performance Ambipolar Polymers Based on Electron-Withdrawing Group Substituted Bay-Annulated Indigo

Jie Yang, Yaqian Jiang, Zeyi Tu, Zhiyuan Zhao, Jinyang Chen, Zhengran Yi, Yifan Li, Shuai Wang,\* Yuanping Yi,\* Yunlong Guo,\* and Yunqi Liu\*

For donor–acceptor conjugated polymers, it is an effective strategy to improve their electron mobilities by introducing electron-withdrawing groups (EWGs, such as F, Cl, or CF<sub>3</sub>) into the polymer backbone. However, the introduction of different EWGs always requires a different synthetic approach, leading to additional arduous work. Here, an effective two-step method is developed to obtain EWG substituted bay-annulated indigo (BAI) units. This method is effective to introduce various EWGs (F, Cl, or CF<sub>3</sub>) into BAI at different substituted positions. Based on this method, EWG substituted BAI acceptors, including 2FBAl, 2ClBAI, and 2CF<sub>3</sub>BAI, are reported for the first time. Furthermore, four polymers of PBAI-V, P2FBAl-V, P2ClBAI-V, and P4OBAI-V are developed. All the polymers show ambipolar transport properties. Particularly, P2ClBAI-V exhibits remarkable hole and electron mobilities of 4.04 and 1.46 cm<sup>2</sup> V<sup>-1</sup> s<sup>-1</sup>, respectively. These mobilities are among the highest values for BAI-based polymers.

the field of low-cost, flexible, and printed optoelectronic devices such as organic photovoltaics (OPVs)<sup>[1]</sup> and organic field-effect transistors (OFETs).<sup>[2]</sup> Currently, the most effective synthetic strategy for high-performance polymers is to design donor–acceptor (D–A) molecular structures.<sup>[3]</sup> There is extensive literature of high-performance p-type D–A polymers based on the well-known units such as diketopyrrolopyrrole (DPP),<sup>[4,5]</sup> isoindigo (IID),<sup>[6]</sup> and benzothiadiazole (BTZ).<sup>[7]</sup> In contrast, the development of ambipolar polymers lags behind that of p-type counterparts due to the lack of strong electron-withdrawing units.<sup>[8,9]</sup> However, ambipolar polymers are of great significance for realizing several important electronic devices, such as complementary metal–oxide–semiconductor (CMOS)-like logic circuits and light-emitting field-effect transistors (LFETs).<sup>[2,10]</sup>

## 1. Introduction

Solution-processable conjugated polymers have attracted increasing attention because of their potential applications in

and light-emitting field-effect transistors (LFETs).<sup>[2,10]</sup>

Most of reported ambipolar or n-type polymers are based on strong electron-withdrawing units such as naphthalenediimide (NDI)<sup>[3]</sup> or benzodifurandione-based oligo(*p*-phenylene vinylene) (BDOPV).<sup>[6]</sup> Introducing EWGs into the polymer backbone is an effective strategy to improve the electron mobilities ( $\mu_e$ ) of the polymers containing moderate electron-deficient units such as DPP, IID, or BTz (Figures S1 and S2, Supporting Information). The introduction of EWGs can effectively lower the lowest unoccupied molecular orbital (LUMO) energy levels of the polymers, which can promote the electron injection and thus improve the  $\mu_e$ . Among these EWGs, F and Cl have been adopted. In fact, high-performance EWG substituted polymers are mostly focused on fluorinated units (Figure S1, Supporting Information), whereas chlorinated polymers are ignored (Figure S2, Supporting Information). In fact, it is fairly difficult to synthesize EWG substituted units, especially for EWG substituted acceptors.<sup>[11]</sup> Substituted acceptors with each different EWG always require a different synthetic approach. For example, the synthetic route to fluorinated IID is noneffective for chlorinated IID, leading to additionally arduous works (Figure S3, Supporting Information).<sup>[12,13]</sup> On the other hand, the mobilities of chlorinated semiconductors are much inferior compared to fluorinated counterparts (Figures S1 and S2, Supporting Information). For example, there is no chlorinated small molecule or polymer with a  $\mu_e$  over 1 cm<sup>2</sup> V<sup>-1</sup> s<sup>-1</sup> due to

J. Yang, Prof. S. Wang  
Key Laboratory of Material Chemistry for Energy  
Conversion and Storage  
Ministry of Education  
School of Chemistry and Chemical Engineering  
Huazhong University of Science and Technology  
Wuhan 430074, China  
E-mail: chmsamuel@hust.edu.cn

J. Yang, Y. Jiang, Dr. Z. Tu, Dr. Z. Zhao, J. Chen, Y. Li,  
Prof. Y. Yi, Prof. Y. Guo, Prof. Y. Liu  
Beijing National Laboratory for Molecular Sciences  
Key Laboratory of Organic Solids  
Institute of Chemistry  
Chinese Academy of Sciences  
Beijing 100190, China  
E-mail: ypyi@iccas.ac.cn; guoyunlong@iccas.ac.cn; liuyq@iccas.ac.cn

Dr. Z. Yi  
School of Chemical Engineering and Pharmacy  
Wuhan Institute of Technology  
Wuhan 430205, China

 The ORCID identification number(s) for the author(s) of this article can be found under <https://doi.org/10.1002/adfm.201804839>.

DOI: 10.1002/adfm.201804839

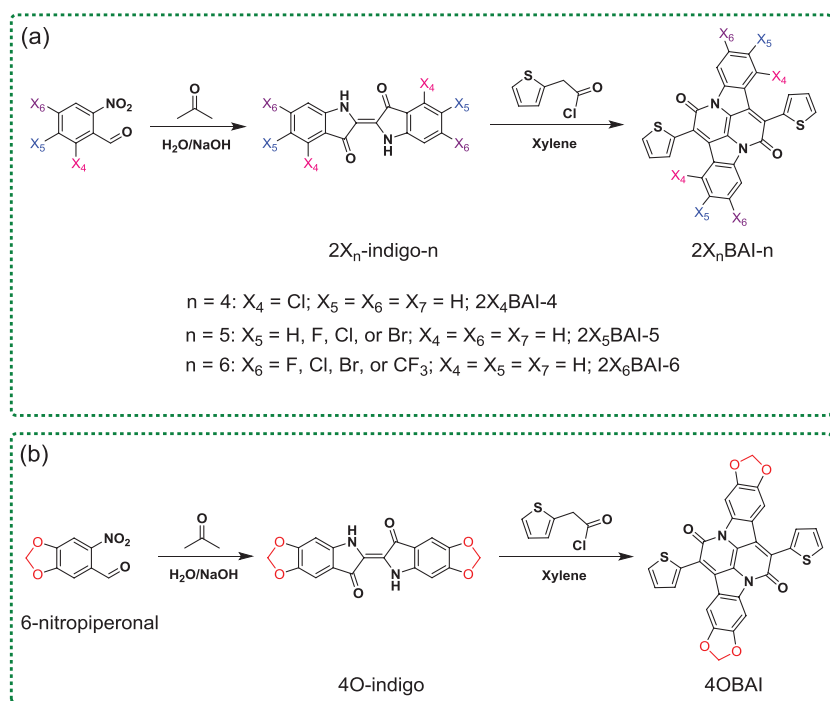


**Figure 1.** An effective two-step approach to different types of BAI acceptors, a) single-substituted BAI derivatives with different substituted positions b) double-substituted BAI derivative (4OBAI).

the steric hindrance effect of big-size Cl atom.<sup>[13,14]</sup> However, we wonder whether high performance can be achieved in a well-designed chlorinated polymer with negligible steric hindrance.

The first bay-annulated indigo (BAI) compound was reported in 1914.<sup>[15]</sup> Recently, Liu and co-workers developed a BAI-based polymer, which showed a hole mobility ( $\mu_h$ ) and  $\mu_e$  of 1.5 and 0.41 cm<sup>2</sup> V<sup>-1</sup> s<sup>-1</sup>, respectively.<sup>[16]</sup> However, the research on BAI-based polymers is still limited.<sup>[16–21]</sup> For example, there is no report of BAI-based polymers with both  $\mu_h$  and  $\mu_e$  over 1.0 cm<sup>2</sup> V<sup>-1</sup> s<sup>-1</sup>. Here, we developed an effective two-step approach (Figure 1) to obtain EWG substituted acceptors based on the BAI unit. This approach was effective to introduce various EWGs (such as F, Cl, or CF<sub>3</sub>) into BAI at different substituted positions. Four polymers of PBAI-V, P2FBAI-V, P2ClBAI-V, and P4OBAI-V were developed by this method. All the polymers showed ambipolar transport behaviors. Particularly, P2ClBAI-V showed a remarkable  $\mu_h/\mu_e$  of 4.04/1.46 cm<sup>2</sup> V<sup>-1</sup> s<sup>-1</sup>. Moreover, we performed theoretical calculations on the effective masses ( $m^*$ ) of the polymers. P2ClBAI-V showed small effective masses, indicating that it is a promising unit for high-performance polymers.

## 2. Results and Discussion

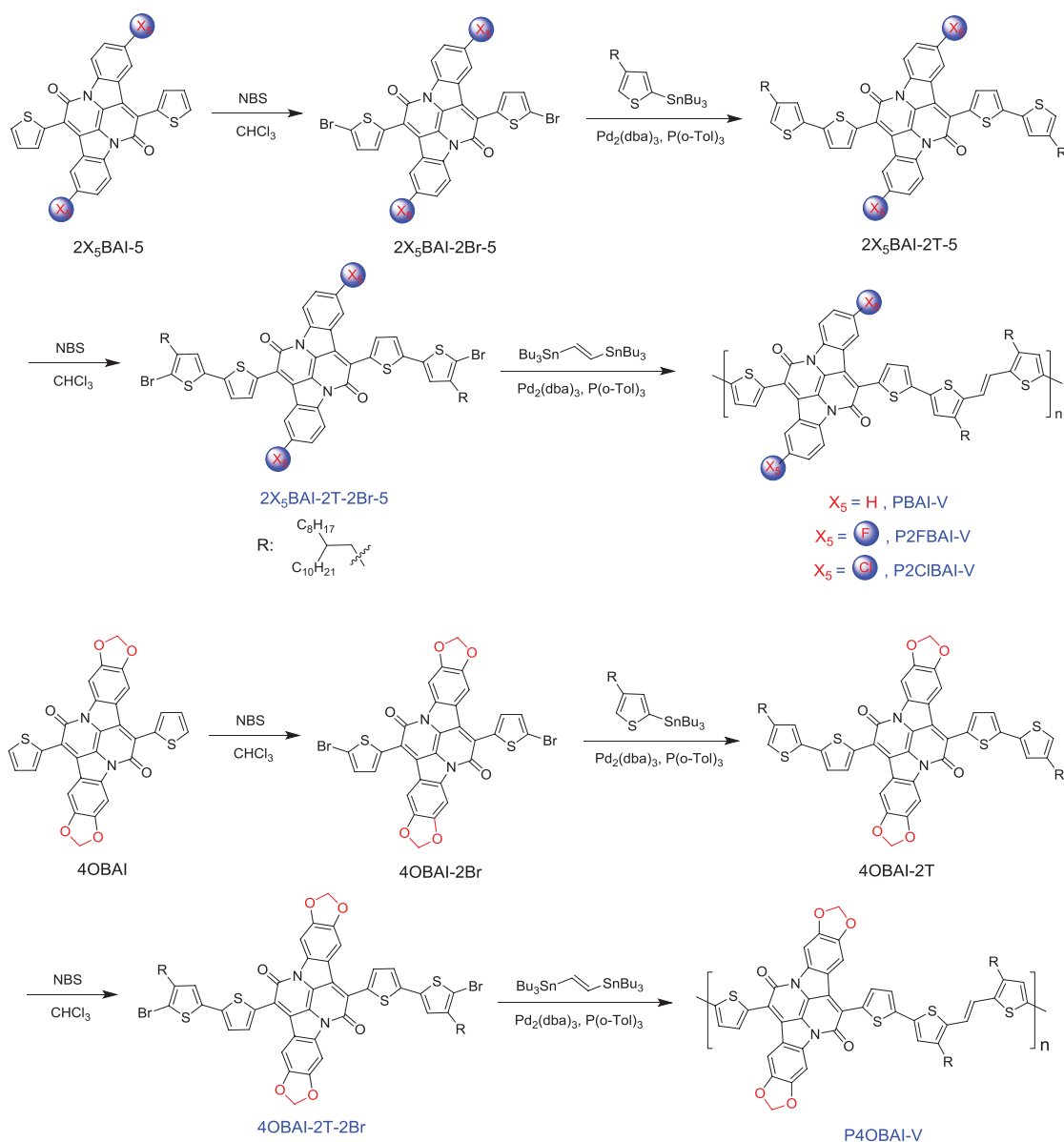
### 2.1. Synthesis

As shown in Figure 1, various substituted BAI derivatives were developed based on an effective two-step method. The two-step approach was composed of two reactions. The first step was synthesis of indigo derivatives. The second step was a one-pot

condensation reaction between indigo derivatives and 2-thienylacetyl chloride. Several routes were developed to synthesize indigo derivatives. For example, three routes to tyrian purple (6,6'-dibromoindigo) were reported (Figure S4, Supporting Information). We selected the simplest route 1 to obtain indigo derivatives. The targeted indigo derivatives were synthesized using commercially available substituted 2-nitrobenzaldehydes as precursors, which reacted with acetone in NaOH aqueous solution. As shown in Table S1 in the Supporting Information, we found that plenty of water and enough reaction time could obviously increase the yield of 2F-indigo-5. To demonstrate the universality of the two-step method, we attempted to synthesize different types of substituted BAI derivatives (Figure 1). 2X<sub>4</sub>BAI-4 was derived from BAI with the 1,8-position substituted by Cl atoms (Figure 1a). 2X<sub>5</sub>BAI-5 was derived from BAI with the 2,9-position substituted by halogen atoms (F, Cl, Br) (Figure 1a). 2X<sub>6</sub>BAI-6 was derived from BAI with the 3,10-position substituted by halogen atoms (F, Cl, Br), or CF<sub>3</sub> (Figure 1a). 2X<sub>4</sub>BAI-4, 2X<sub>5</sub>BAI-5, and 2X<sub>6</sub>BAI-6 were all single-substituted BAI derivatives. 4OBAI was derived

from BAI with dioxolane rings fused to the benzene rings (Figure 1b). 4OBAI was an example among the double-substituted derivatives of BAI although the dioxolane ring was an electron-donating group. Interestingly, the synthesis of 4OBAI started from piperonal (Supporting Information), which is a natural product existing in some plants such as pepper and saffras. We successfully synthesized ten BAI derivatives by the two-step approach, demonstrating it was a general method.

Bromination of 2FBAI-5 using *N*-bromosuccinimide (NBS) in chloroform yielded 2FBAI-2Br-5 in 71% yield, which underwent Stille coupling with 3-(2-octyldodecyl)-5-tributylstannylthiophene to give 2FBAI-2T-5. Unfortunately, the Stille coupling reaction showed moderate yield (<30%) due to the poor solubility of 2FBAI-2Br-5 in the reaction solution. As shown in Table S1 in the Supporting Information, we conducted the Stille coupling reaction in different solvents. Similar yields (about 11%) were found in toluene and toluene/DMF (v/v, 4:1). Higher yield (15.2%) was achieved in chlorobenzene. In *o*-dichlorobenzene, the reaction showed the highest yield of 21.7%. Other soluble products, BAI-2T, 2ClBAI-2T-4, 2ThBAI-5, 2ClBAI-2T-5, 2ClBAI-2T-6, 2FBAI-2T-6, and 4OBAI-2T were synthesized following the similar procedures as 2FBAI-2T-5. From the eight soluble BAI derivatives, we selected 2FBAI-2T-5, BAI-2T, 2ClBAI-2T-5, and 4OBAI-2T to further develop their monomers and polymers (Scheme 1). Bromination of above four products gave the corresponding monomers. Stille coupling polymerization between the four monomers and *trans*-1,2-bis(tributylstannyl)ethene afforded the corresponding polymers. Vinyl group was selected as the donor because it could form a coplanar molecular structure with the adjacent alkylated thiophenes (Figure S23, Supporting Information).



**Scheme 1.** An effective route to four BAI-based monomers and polymers.

We conducted solubility tests (Figure S6, Supporting Information) of the polymers in common chlorinated solvents. PBAI-V, P2ClBAI-V, and P4OBAI-V showed good solubility in chloroform ( $\approx 25 \text{ mg mL}^{-1}$ ), chlorobenzene ( $\approx 15 \text{ mg mL}^{-1}$ ), and *o*-dichlorobenzene ( $\approx 15 \text{ mg mL}^{-1}$ ). However, the fluorinated polymer, P2FBAI-V showed inferior solubility in chloroform ( $\approx 10 \text{ mg mL}^{-1}$ ) and was hardly soluble ( $< 3 \text{ mg mL}^{-1}$ ) in chlorobenzene and *o*-dichlorobenzene. The results indicated that fluorination of polymers decreased the solubility in chlorinated solvents. As shown in **Table 1**, number-average molecular weights ( $M_n$ ) of PBAI-V, P2FBAI-V, P2ClBAI-V, and P4OBAI-V were 25.2, 17.9, 32.5, and 18.0 kDa, respectively. Thermogravimetric analysis (TGA) curves indicated that the polymers exhibited good thermal stability (Figure S7, Supporting Information).

## 2.2. Optical and Electrochemical Properties

The UV-vis absorption spectra of the polymers were measured both in chloroform solution and in thin film. As shown in **Figure 2**, the polymers showed broad absorption bands from 600 to 1100 nm, which were attributed to the  $\pi$ - $\pi^*$  transitions and the intramolecular charge transfer (ICT).<sup>[22,23]</sup> As shown in Figure S6 in the Supporting Information, all the BAI-based polymers were green in solution, similar to DPP-based polymers. The absorption maxima ( $\lambda_{\text{max}}$ ) of P2ClBAI-V in chloroform solution and in film red shifted compared to those of PBAI-V. For instance, the  $\lambda_{\text{max}}$  of solution increased from 827 nm for PBAI-V to 918 nm for P2ClBAI-V. The red shift of  $\lambda_{\text{max}}$  could be attributed to the enhanced “push-pull” interactions between the 2ClBAI and neighboring thiophenes

**Table 1.** Number average molecular weights, polydispersity index (PDI), wavelength of absorption maxima, bandgaps, HOMO, and LUMO energy levels of the polymers.

Polymer	$M_n$ [kDa]/PDI	$\lambda_{\max}$ [nm]	$E_g^{\text{opt a)}$ [eV]	HOMO <sup>b)</sup> [eV]	LUMO <sup>b)</sup> [eV]
PBAI-V	25.2/2.03	827 <sup>c)</sup> /794 <sup>d)</sup>	1.16	-5.22	-3.65
P2FBAl-V	17.9/1.83	699/714	1.15	-5.58	-3.72
P2ClBAI-V	32.5/1.93	918/897	1.04	-5.32	-3.70
P4OBAI-V	18.0/1.82	785/773	1.19	-5.16	-3.57

<sup>a)</sup>Determined from the onset of thin-film absorption; <sup>b)</sup>Determined from the onset of oxidation and reduction potentials of cyclic voltammetry; <sup>c)</sup>Absorption maximum in chloroform solution; <sup>d)</sup>Absorption maximum in film.

because 2ClBAI was more electron-deficient than BAI.<sup>[24]</sup> Similarly, P4OBAI-V showed blue-shift  $\lambda_{\max}$  compared to PBAI-V due to the electron-donating characteristic of substituted dioxolane rings. However, the  $\lambda_{\max}$  of P2FBAl-V in solution blue shifted to 699 nm after introducing fluorine atoms, which was unusual and needed further studies. As shown in Table 1, all the polymers showed narrow film optical bandgaps ( $E_g^{\text{opt}}$ ) of about 1.2 eV. In particular, P2ClBAI-V exhibited a  $E_g^{\text{opt}}$  of 1.04 eV, which was among the smallest values for the reported D–A polymers.<sup>[3]</sup> In addition, temperature-dependent UV–vis absorption spectra of the polymers in chlorobenzene solution were performed to investigate aggregation property of each polymer (Figure S8, Supporting Information). Upon increasing solution temperature, the  $\lambda_{\max}$  at ICT band of PBAI-V, P2ClBAI-V, and P4OBAI-V only showed slight blue shifts (<10 nm), indicating that the polymers exhibited weak aggregation in chlorobenzene solution.<sup>[25,26]</sup> Meanwhile, the  $\lambda_{\max}$  of P2FBAl-V showed no obvious change at different temperatures.

The electrochemical properties of the polymers were evaluated by cyclic voltammetry (CV) (Figure S9, Supporting Information). All the polymers exhibited intense oxidative and reductive peaks. The highest occupied molecular orbital (HOMO) and LUMO energy levels of the polymers were calculated from the onsets of oxidative and reductive peaks, respectively. The HOMO and LUMO energy levels of PBAI-V were -5.22 and -3.65 eV, respectively. Fluorination and chlorination can lower both the HOMO and LUMO energy levels due to the electron-withdrawing characteristics of F and Cl atoms. For instance, the LUMO energy levels of P2FBAl-V and P2ClBAI-V decreased to -3.72 and -3.70 eV, respectively. Notably, P2FBAl-V showed a deep HOMO energy level of

-5.58 eV. The HOMO and LUMO energy levels of P4OBAI-V increased to -5.16 and -3.57 eV compared to PBAI-V due to the electron-donating characteristic of substituted dioxolane rings.

### 2.3. Field-Effect Transistor Devices

Field-effect transistors (FETs) with top-gate bottom-contact (TGBC) configuration were fabricated on glass substrates to investigate the carrier transport properties of the polymers. The device configuration of TGBC OFETs is shown in Figure S10 in the Supporting Information. Gold source/drain electrodes and aluminum gate electrodes were thermally evaporated via a shadow mask. Polymethyl methacrylate (PMMA) served as a dielectric layer. For OFETs based on PBAI-V, P2ClBAI-V, and P4OBAI-V, the semiconducting layers were spin-coated from *o*-dichlorobenzene solutions. In comparison, P2FBAl-V was processed in chloroform solution due to its poor solubility in *o*-dichlorobenzene (Figure S6, Supporting Information). The fabrication procedures of FET devices are provided in the Experimental Section. As shown in Table S2 in the Supporting Information, P2ClBAI-V showed the highest mobilities when annealed at 180 °C, which was determined as the optimal annealing temperature. Figure 3 and Figures S11–S13 (Supporting Information) show the output and transfer curves of the annealed polymers. Saturation mobilities were extracted using  $I_{\text{DS}}$  square root dependence on gate voltage ( $V_G$ ) under  $V_{\text{DS}}$  of  $\pm 60$  V. As shown in Figures S14–S17 in the Supporting Information, the mobilities extracted from the transfer curves of all the polymers showed weak dependence on  $V_G$ .<sup>[27]</sup>

All the polymers showed ambipolar transport behaviors with typical V-shaped transfer curves (Figure 3 and Figures S11–S13, Supporting Information). The carrier mobilities, threshold voltages, and on/off current ratios were extracted from the transfer curves in the saturation regimes and were shown in Table 2. We calculated reliability factors of saturated mobility for the polymers to ensure the reliability of mobility data.<sup>[27]</sup> PBAI-V showed ambipolar performance with a maximum  $\mu_h/\mu_e$  of 1.30/0.34  $\text{cm}^2 \text{V}^{-1} \text{s}^{-1}$ . In contrast, P2FBAl-V was almost an n-type semiconductor with a  $\mu_e$  of

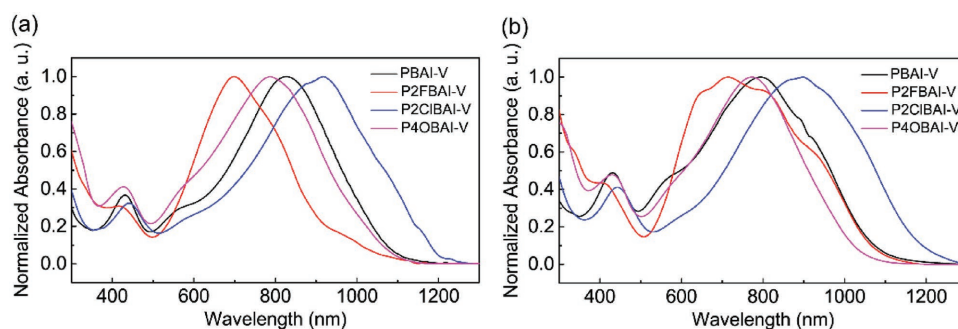


**Figure 2.** UV–vis absorption spectra of the polymers a) in chloroform solution and b) in thin film.

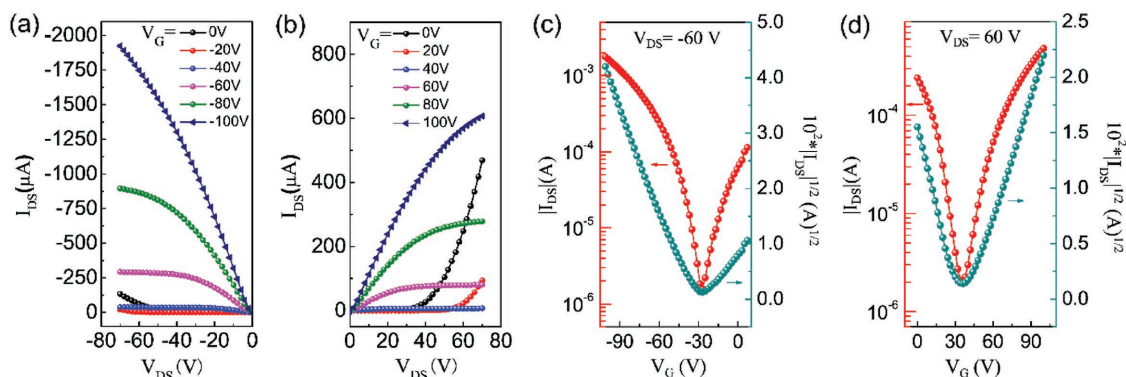


**Figure 3.** a,b) Output and c,d) transfer characteristics of a TGBC device based on P2ClBAI-V.

0.16 cm<sup>2</sup> V<sup>-1</sup> s<sup>-1</sup> and a negligible  $\mu_h$  of 10<sup>-4</sup> cm<sup>2</sup> V<sup>-1</sup> s<sup>-1</sup>. The HOMO energy level of P2FBAI-V was -5.58 eV, which was unfavorable for hole injection from the Au electrodes (work function ≈5.1 eV).<sup>[28]</sup> Interestingly, the chlorinated polymer, P2ClBAI-V showed significantly improved performance with a  $\mu_h/\mu_e$  of 4.04/1.46 cm<sup>2</sup> V<sup>-1</sup> s<sup>-1</sup>. These mobilities were among the highest values for BAI-based polymers and were comparable to those of well-known DPP-based polymers.<sup>[16,18,29]</sup> P4OBAI-V showed inferior performance with  $\mu_h$  and  $\mu_e$  of 0.17 and 0.085 cm<sup>2</sup> V<sup>-1</sup> s<sup>-1</sup>, respectively. In addition, we fabricated bottom-gate bottom-contact (BGBC) devices based on P2ClBAI-V. Highly-doped SiO<sub>2</sub>/Si wafers were used as substrates. The SiO<sub>2</sub> surface was modified with octadecyltrichlorosilane (OTS) to minimize surface charge trapping. As shown in Figure S18 in the Supporting Information, P2ClBAI-V based BGBC devices showed ambipolar performance with a maximum  $\mu_h/\mu_e$  of 1.06/0.53 cm<sup>2</sup> V<sup>-1</sup> s<sup>-1</sup> in nitrogen atmosphere. Compared with the TGBC devices, the inferior performance for the BGBC devices was attributed to charge trapping at the interface between the semiconductor and the silicon dioxide dielectric.<sup>[18,30,31]</sup> We further evaluated the performance of BAI-based polymers by comparing them with the reported DPP and IID-based polymers. PBAI-V, PDPP-(E)-2-(2-(thiophen-2-yl)vinyl)thiophene (TVT), and PIID-TVV were selected as the targeted polymers because all of them contained similar TVT donors (Figure S19, Supporting Information). PDPP-TVV and PIID-TVV were nearly unipolar p-type polymers.<sup>[29,30]</sup> In comparison, PBAI-V showed obvious n-type performance with a  $\mu_e$  of 0.34 cm<sup>2</sup> V<sup>-1</sup> s<sup>-1</sup> due to its lowest LUMO energy level (-3.65 eV) among the three polymers. Therefore, BAI units would be promising building blocks for ambipolar polymers.

## 2.4. Film Crystallinity and Morphology

2D grazing incident X-ray diffractions (2D-GIXRD) were conducted to explore the crystalline nature of the polymers. 2D-GIXRD patterns of annealed films at 180 °C on glass substrates are shown in **Figure 4**. For all the polymers, (h00) diffraction peaks corresponding to lamellar diffractions were observed along the in-plane ( $q_{xy}$ ) and out-of-plane ( $q_z$ ) directions.

The out-of-plane (100) diffraction of PBAI-V was found at  $2\theta = 4.64^\circ$ , corresponding to a lamellar  $d$ -spacing of 19.0 Å. Similarly, the lamellar  $d$ -spacings of P2FBAI-V, P2ClBAI-V, and P4OBAI-V were 20.4, 19.9, and 19.7 Å, respectively. For all the polymers, (010) diffraction peaks corresponding to the  $\pi$ - $\pi$  stacking were observed along the out-of-plane and in-plane direction (Figure S20, Supporting Information), suggesting that the  $\pi$ - $\pi$  stacking crystallites adopted a bimodal distribution of edge-on and face-on orientations. PBAI-V, P2ClBAI-V, and P4OBAI-V showed  $\pi$ -stacking spacings of 3.53, 3.54, and 3.52 Å, respectively, which were calculated from the (010) diffraction peaks. The  $\pi$ -stacking spacings of the three polymers were among the smallest values for D-A polymers,<sup>[4]</sup> promising effective intermolecular charge transport for carriers. The comparative  $\pi$ -stacking spacings of PBAI-V and P2ClBAI-V indicated that chlorination of BAI did not cause obvious steric hindrance to hinder the intermolecular stacking although the chlorine atom has a large atom size.<sup>[13]</sup> Surprisingly, P2FBAI-V showed a much larger  $\pi$ -stacking spacing of 3.68 Å than the other three polymers. Different from DPP or IID-based polymers,<sup>[4,6]</sup> these BAI-based polymers exhibited (00 $l$ ) diffraction peaks, which corresponded to planes resulting from repeat polymer units in

**Table 2.** TGBC OFET performance of the polymers.

Polymer	$\mu_h^b$ [cm <sup>2</sup> V <sup>-1</sup> s <sup>-1</sup> ]	p-type			$\mu_e^b$ [cm <sup>2</sup> V <sup>-1</sup> s <sup>-1</sup> ]	n-type			p/n ratio <sup>a)</sup>
		$r_{sat}^c$	$V_{th}^d$ [V]	$I_{on}/I_{off}^e$		$r_{sat}^c$	$V_{th}^d$ [V]	$I_{on}/I_{off}^e$	
PBAI-V	1.30 (0.94)	0.561	-33 (±2)	10 <sup>3</sup> -10 <sup>4</sup>	0.34 (0.28)	0.759	58 (±3)	10 <sup>2</sup> -10 <sup>3</sup>	3.36
P2FBAI-V	8.4 × 10 <sup>-4</sup> (6.7 × 10 <sup>-4</sup> )	0.854	-14 (±4)	10 <sup>2</sup> -10 <sup>3</sup>	0.16 (0.12)	0.718	43 (±5)	10 <sup>3</sup> -10 <sup>4</sup>	5.6 × 10 <sup>-3</sup>
P2ClBAI-V	4.04 (2.82)	0.691	-36 (±4)	10 <sup>2</sup> -10 <sup>3</sup>	1.46 (1.01)	0.734	39 (±4)	10 <sup>2</sup> -10 <sup>3</sup>	2.79
P4OBAI-V	0.17 (0.15)	0.508	-24 (±1)	10 <sup>3</sup> -10 <sup>4</sup>	0.085 (0.037)	0.757	66 (±4)	10 <sup>2</sup> -10 <sup>3</sup>	4.05

<sup>a)</sup>Ratio of average hole and electron mobility; <sup>b)</sup>Maximum mobilities extracted from the transfer curves in the saturation regimes. The average values are listed in parentheses. The mobility values were calculated from the high gate voltage region; <sup>c)</sup> $r_{sat}$  represents reliability factor of saturated mobility; <sup>d)</sup>Threshold voltage; <sup>e)</sup>On-off current ratio.

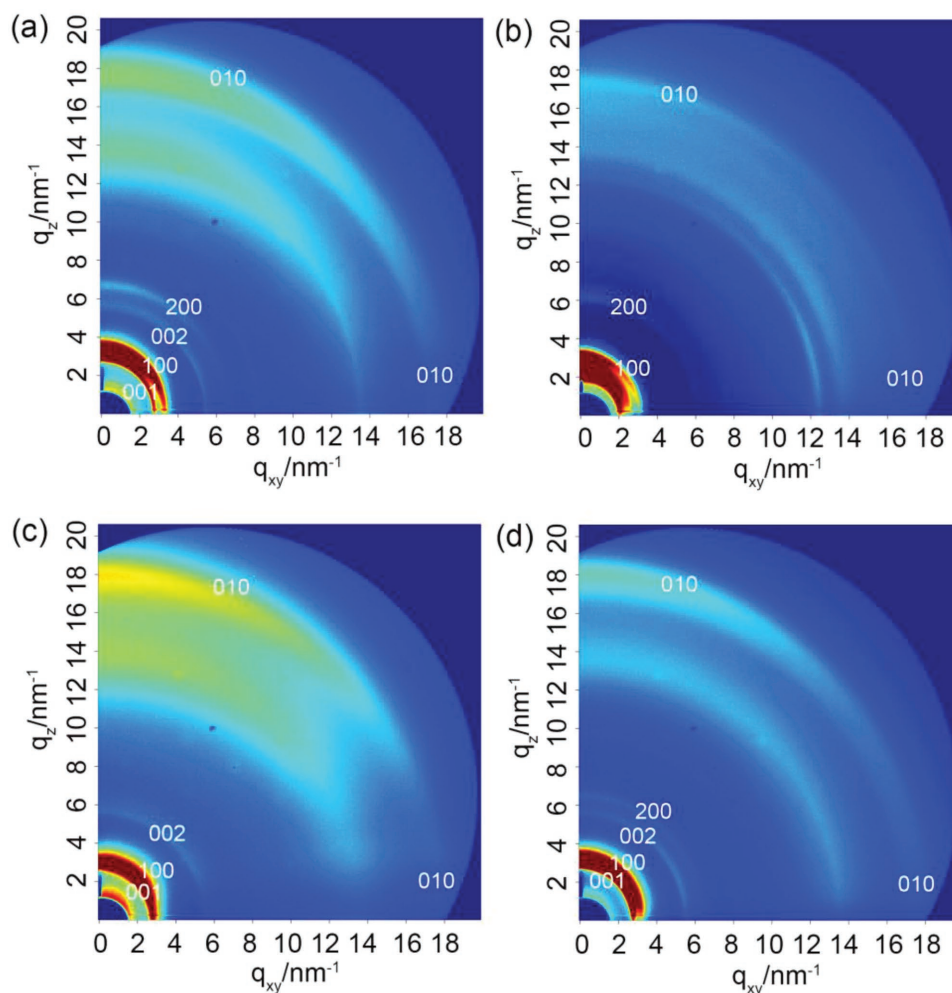


**Figure 4.** 2D-GIXRD patterns of a) PBAI-V, b) P2FBAI-V, c) P2ClBAI-V, and d) P4OBAI-V films annealed at 180 °C.

an ordered mainchain backbone.<sup>[18,19]</sup> All the polymers except P2FBAI-V showed (001) and (002) diffraction peaks. PBAI-V, P2ClBAI-V, and P4OBAI-V showed close (001) *d*-spacings of 22.43, 22.60, and 22.37 Å, respectively. The theoretical calculated length of a repeat unit of each polymer was almost the same ( $\approx 22.67$  Å) (Figure S23, Supporting Information). The backbone-direction (001) *d*-spacing of each polymer was very close to the theoretical calculated length of a repeat unit, indicating that the polymer backbone should be entirely extended (not twisted) along the conjugated direction in solid state, thus resulting in better intramolecular charge transport characteristics.<sup>[18,32]</sup>

Figures S21 and S22 in the Supporting Information show the atomic force microscopy (AFM) images of annealed polymer films on glass substrates. All the polymer films showed well-interconnected domains that could minimize the intergranular charge hopping barriers. The films of all the polymers except P2FBAI-V exhibited relatively low root-mean-square (RMS) surface roughness of below 1 nm. Particularly, P2ClBAI-V showed fairly smooth interface with a small RMS of 0.12 nm. The smooth interface was beneficial for charge transport in top-gate OFETs, consistent with the results in reported high-performance ambipolar polymers.<sup>[33]</sup>

## 2.5. Theoretical Calculations

Charge transport in semiconducting polymers includes intramolecular charge transport along the conjugated backbone and intermolecular charge transport through  $\pi$ - $\pi$  stacking. It is difficult to evaluate intramolecular charge transport by experimental methods, which plays an important role in high-mobility polymers. Recently, we introduced the concept “ $m^*$ ” to evaluate intramolecular charge transport, where a small  $m^*$  reveals effective intramolecular charge transport.<sup>[34]</sup> The  $m^*$  can be obtained by theoretical calculations. Here, we calculated the  $m^*$  of the four polymers based on their simulative 1D crystalline structures. Figure S23 in the Supporting Information shows the planarity data of the polymers. All the polymers showed similar planarity with the maximum torsion angles between the BAI core and adjacent thiophenes being about 27°, which was comparable to IID-based polymers ( $\approx 22^\circ$ )<sup>[12]</sup> but smaller than NDI-based counterparts ( $\approx 40^\circ$ ).<sup>[35]</sup> Notably, the large-size chlorine atoms in P2ClBAI-V did not lead to worse planarity. Figure 5d–g shows the calculated band structures and densities of states (DOS). Hole and electron effective masses ( $m_h^*$  and  $m_e^*$ ) of the polymers were calculated based on the

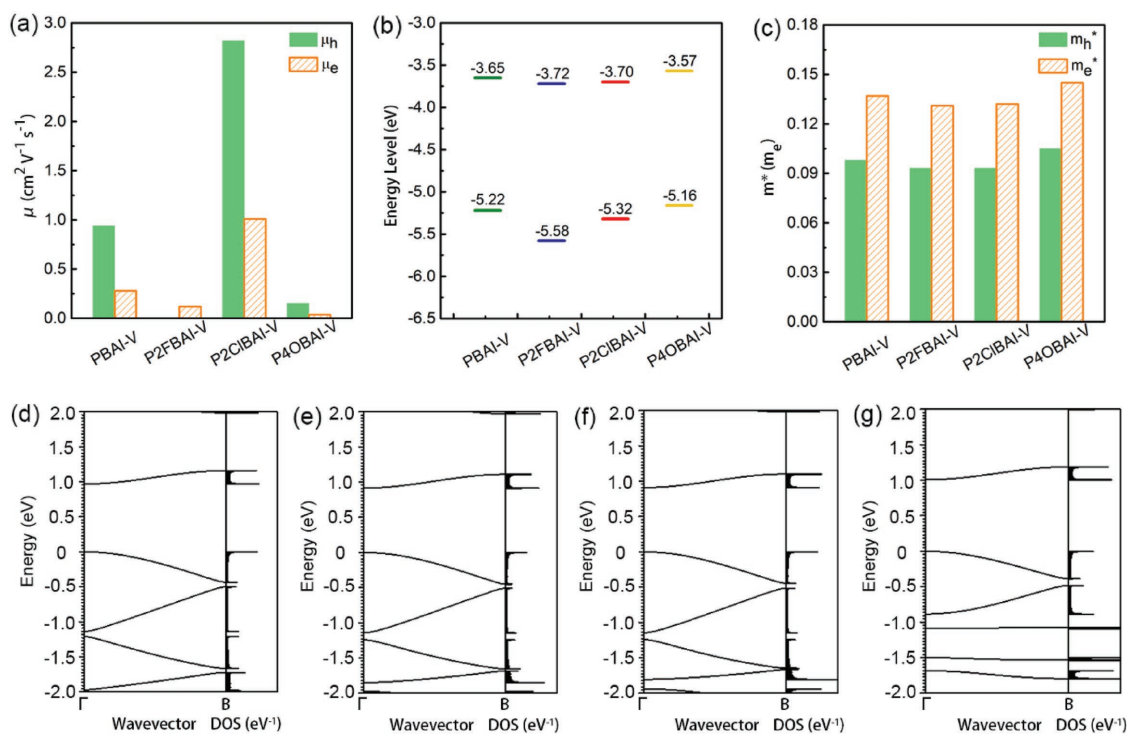


**Figure 5.** a) Average hole and electron mobilities of the polymers extracted from the transfer curves. b) HOMO and LUMO energy levels of the polymers determined from CV. c) Hole and electron effective masses ( $m_h^*$  and  $m_e^*$ ) obtained from the theoretical calculations. Band structures and partial density of states (DOS) of d) PBAI-V, e) P2FBAl-V, f) P2ClBAI-V, and g) P4OBAI-V.

second derivative of band structures. As shown in Table 2, all the polymers showed small  $m_h^*$  and  $m_e^*$ . PBAI-V showed small  $m_h^*$  and  $m_e^*$  of 0.098 and 0.137  $m_e$ , respectively. In comparison, P2FBAl-V and P2ClBAI-V showed slightly smaller  $m_h^*$  and  $m_e^*$ , indicating that both fluorination and chlorination of the BAI could promote more effective intramolecular charge transport. P4OBAI-V showed much larger  $m_h^*$  and  $m_e^*$  than those of PBAI-V. Table S5 in the Supporting Information shows calculated  $m^*$  of IID and NDI-based polymers. We noted that P2FBAl-V and P2ClBAI-V showed comparable  $m^*$  to IID-based polymers but much smaller  $m^*$  than NDI-based counterparts. The results revealed that the intramolecular charge transport in P2FBAl-V or P2ClBAI-V was as effective as in IID-based counterparts. In consideration that IID unit was a well-known acceptor for high-mobility polymers, we believed that 2FBAl or 2ClBAI would be a promising building block for high-performance ambipolar polymers.

Here, we tried to explain the trend of the polymers' mobilities from the aspects of charge injection and transport based on above results of CV, GIXRD, and AFM. P2FBAl-V showed inferior performance, which could be attributed to its inferior solubility in chloroform. Similar phenomena could be found in BDOPV-based polymers.<sup>[36,37]</sup> Moreover, P2FBAl-V showed bad crystallinity with weak ( $h00$ ) and (010) peaks and a large  $\pi$ -stacking spacing of 3.68 Å, indicating inferior intermolecular charge transport in P2FBAl-V. We are attempting to design other 2FBAl-based polymers with good solubility for better device performance. Compared with PBAI-V, P2ClBAI-V showed improved hole and electron mobilities. Several reasons were responsible for the results: 1) P2ClBAI-V showed lower

LUMO energy level than PBAI-V (Figure 5b), thus promoting the electron injection. 2) GIXRD results indicated that chlorination of BAI did not cause obvious steric hindrance to hinder the intermolecular stacking. 3) Different from F atom, Cl atom has empty 3d orbitals, which can accept  $\pi$ -electrons from the donors. As a result, strong intermolecular interactions would form in chlorinated polymers, which can modulate their film crystallinity or morphology.<sup>[38–40]</sup> AFM results indicated that P2ClBAI-V showed more smooth interface compared with PBAI-V. The smoother interface was beneficial for better charge transport in top-gate OFETs.<sup>[33]</sup>

### 3. Conclusion

In conclusion, we developed a general two-step method to obtain EWG substituted acceptors based on BAI units. This method was effective to introduce various EWGs (such as F, Cl, or  $\text{CF}_3$ ) into BAI at different substituted positions. Four new polymers of PBAI-V, P2FBAl-V, P2ClBAI-V, and P4OBAI-V were developed by this approach. All the polymers showed ambipolar transport behaviors. Particularly, P2ClBAI-V exhibited remarkable performance with a  $\mu_h/\mu_e$  of 4.04/1.46  $\text{cm}^2 \text{V}^{-1} \text{s}^{-1}$ . These mobilities were the best values achieved for chlorinated semiconductors (including small molecules and polymers). Theoretical calculations and GIXRD indicated that the introduction of Cl atoms in P2ClBAI-V did not distort the backbone coplanarity and not hinder the  $\pi$ - $\pi$  stacking. For the first time, our results demonstrate that chlorination can be a promising strategy for high-performance ambipolar polymers. Moreover,

the effective two-step approach can achieve various EWG substituted BAI acceptors, which will significantly enrich the library of ambipolar polymers.

## 4. Experimental Section

**Characterization:** Nuclear magnetic resonance (NMR) spectra were recorded on a Bruker DMX-300 (300 MHz) spectrometer. <sup>1</sup>H NMR chemical shifts were referenced to internal tetramethylsilane (TMS, 0 ppm). High-resolution mass spectroscopy (HRMS) measurements were collected using electron-impact mass spectra (EIMS) on a Bruker BIFLEX III mass spectrometer. Matrix-assisted laser desorption/ionization time-of-flight (MALDI-TOF) mass spectra were collected on an Autoflex III (Bruker Daltonics Inc.) MALDI-TOF spectrometer. Molecular weights were determined by gel permeation chromatography (GPC) at 120 °C on a PL-220 system using 1,2,4-trichlorobenzene as the eluent. TGA measurements were carried out on a PerkinElmer series 7 thermal analysis system under N<sub>2</sub> at a heating rate of 10 °C min<sup>-1</sup>. UV-vis absorption spectra were measured on polymer solutions in chloroform and polymer films cast onto quartz glass using a Jasco-570 spectrophotometer. CV was carried out on an electrochemical workstation (CHI660c) using a three-electrode cell. The glassy carbon electrode coated with a thin film layer of polymer was used as working electrode. Ag/AgCl (Ag in a 0.01 mol L<sup>-1</sup> KCl) electrode was used as the reference electrode. Platinum wire was used as the counter electrode. Anhydrous and N<sub>2</sub> saturated solution 0.1 M tetrabutylammonium hexylfluorophosphate (*n*-Bu<sub>4</sub>NPF<sub>6</sub>) in acetonitrile was employed as the electrolyte. AFM measurements were carried out on a Nanoscope V instrument. AFM samples were identical to those used in FET performance analysis. GIXRD was performed on 1W1A Station of Beijing Synchrotron Radiation Facility ( $\lambda = 1.5418 \text{ \AA}$ ).

**Polymer Synthesis:** PBAI-V: BAI-2T-2Br (100.0 mg, 0.074 mmol), *trans*-1,2-bis(tributylstannyl)ethene (44.6 mg, 0.074 mmol), Pd<sub>2</sub>(dba)<sub>3</sub> (2.0 mg), P(*o*-tol)<sub>3</sub> (5.2 mg), and chlorobenzene (6 mL) were added to a Schlenk tube. The tube was charged with argon through a freeze-pump-thaw cycle for three times. The mixture was stirred for 48 h at 130 °C, cooled down to room temperature, and poured into methanol (100 mL) containing hydrochloric acid (5 mL) and stirred for 3 h. The precipitated product was filtered and purified via Soxhlet extraction with methanol (10 h), acetone (10 h), hexane (10 h), and was finally collected with chloroform. The chloroform fraction was concentrated by evaporation and precipitated into methanol (100 mL) and filtered off to afford the green polymer (85.2 mg, 94.6%). GPC:  $M_n = 25.2 \text{ kDa}$ ,  $M_w = 46.3 \text{ kDa}$ , polydispersity index (PDI) = 2.03. Anal. calcd. for C<sub>78</sub>H<sub>98</sub>N<sub>2</sub>O<sub>2</sub>S<sub>4</sub>: C 76.55, H 8.07, N 2.29; found: C 74.74, H 8.00, N 2.27.

P2FBAI-V: 2FBAI-2T-2Br-5 (200.0 mg, 0.144 mmol), *trans*-1,2-bis(tributylstannyl)ethene (87.0 mg, 0.144 mmol), Pd<sub>2</sub>(dba)<sub>3</sub> (3.9 mg), P(*o*-tol)<sub>3</sub> (10.5 mg), and toluene (12 mL) were added to a Schlenk tube. The tube was charged with argon through a freeze-pump-thaw cycle for three times. The mixture was stirred at 110 °C for several minutes (about 4 min) before being gelled, cooled down to room temperature, and poured into methanol (200 mL) containing hydrochloric acid (10 mL) and stirred for 3 h. The precipitated product was filtered and purified via Soxhlet extraction with methanol (10 h), acetone (10 h), hexane (10 h), chloroform (10 h), chlorobenzene (5 h), and finally *o*-dichlorobenzene (5 h). The chlorinated fractions were concentrated by evaporation and precipitated into methanol (200 mL) and filtered off to afford the green polymers: chloroform fraction (81.2 mg, 45.0%), chlorobenzene fraction (very less), *o*-dichlorobenzene fraction (very less). GPC:  $M_n = 17.9 \text{ kDa}$ ,  $M_w = 29.9 \text{ kDa}$ , PDI = 1.83. Anal. calcd. for C<sub>78</sub>H<sub>96</sub>F<sub>2</sub>N<sub>2</sub>O<sub>2</sub>S<sub>4</sub>: C 74.36, H 7.68, N 2.22; found: C 69.91, H 7.23, N 2.18.

P2CIBAI-V: 2CIBAI-2T-2Br-5 (100.0 mg, 0.070 mmol), *trans*-1,2-bis(tributylstannyl)ethene (42.5 mg, 0.070 mmol), Pd<sub>2</sub>(dba)<sub>3</sub> (2.0 mg), P(*o*-tol)<sub>3</sub> (5.2 mg), and chlorobenzene (6 mL) were added to a Schlenk tube. The tube was charged with argon through a freeze-pump-thaw cycle for three times. The mixture was stirred for 48 h at 130 °C. The

next purification of the polymer was similar to PBAI-V. The chloroform fraction was concentrated by evaporation and precipitated into methanol (100 mL) and filtered off to afford the green polymer (79.4 mg, 87.5%). GPC:  $M_n = 32.5 \text{ kDa}$ ,  $M_w = 57.2 \text{ kDa}$ , PDI = 1.93. Anal. calcd. for C<sub>78</sub>H<sub>96</sub>Cl<sub>2</sub>N<sub>2</sub>O<sub>2</sub>S<sub>4</sub>: C 72.47, H 7.49, N 2.17; found: C 71.46, H 7.55, N 2.15.

P4OBAI-V: 4OBAI-2T-2Br (100.0 mg, 0.069 mmol), *trans*-1,2-bis(tributylstannyl)ethene (41.9 mg, 0.069 mmol), Pd<sub>2</sub>(dba)<sub>3</sub> (2.0 mg), P(*o*-tol)<sub>3</sub> (5.2 mg), and toluene (6 mL) were added to a Schlenk tube. The tube was charged with argon through a freeze-pump-thaw cycle for three times. The mixture was stirred for 24 h at 110 °C. The next purification of the polymer was similar to PBAI-V. The chloroform fraction was concentrated by evaporation and precipitated into methanol (100 mL) and filtered off to afford the green polymer (52.3 mg, 57.6%). GPC:  $M_n = 18.0 \text{ kDa}$ ,  $M_w = 29.6 \text{ kDa}$ , PDI = 1.82. Anal. calcd. for C<sub>80</sub>H<sub>98</sub>N<sub>2</sub>O<sub>6</sub>S<sub>4</sub>: C 73.24, H 7.53, N 2.14; found: C 72.48, H 7.57, N 2.16.

**TGBC OFET Fabrication and Characterization:** Polymer FETs with a TGBC configuration were fabricated on Corning glass substrates. The substrates were rinsed by deionized water, ethanol, acetone under ultrasonication and dried by nitrogen before device fabrication. The source-drain gold electrodes were prepared by vacuum evaporation technique. The channel width and length of all FET devices were 4500 and 50  $\mu\text{m}$ , respectively. PBAI-V, P2CIBAI-V, and P4OBAI-V were dissolved in 1,2-dichlorobenzene (10 mg mL<sup>-1</sup>). P2FBAI-V was dissolved in chloroform (10 mg mL<sup>-1</sup>). In a nitrogen glovebox, the polymer solutions were spin-coated onto the substrates, yielding polymer films. Then the film samples were further annealed at 180 °C for 10 min. Next, PMMA ( $M_w = 996 \text{ kDa}$ ) solution in anhydrous *n*-butyl acetate (60 mg mL<sup>-1</sup>) was spin-coated onto the surface of the polymer films (PMMA thickness  $\approx 900 \text{ nm}$ , capacitance  $\approx 2.56 \text{ nF cm}^{-2}$ ).<sup>[41]</sup> The samples were dried at 90 °C for 50 min in glove box. Finally, the aluminum gate electrodes (thickness  $\approx 80 \text{ nm}$ ) were evaporated onto PMMA through a shadow mask. All the FET devices were determined under the ambient conditions using a Keithley 4200 SCS semiconductor parameter analyzer. The field-effect mobility in saturation region ( $\mu_{\text{sat}}$ ) is calculated according to the Equation (1)

$$I_{\text{DS}} = (W/2L)C_i\mu_{\text{sat}}(V_G - V_{\text{th}})^2 \quad (1)$$

where  $I_{\text{DS}}$  is the drain current;  $W$  and  $L$  are the semiconductor channel width and length, respectively;  $C_i$  is the capacitance per unit area of the gate dielectric layer; and  $V_G$  and  $V_{\text{th}}$  are the gate voltage and threshold voltage, respectively.

**BGBC OFET Fabrication and Characterization:** BGBC FETs were fabricated on highly-doped silicon wafer with 300 nm SiO<sub>2</sub> insulator. Silicon was used as bottom gate electrode. The gold (gold/titanium, 30 nm/5 nm) electrodes were served as source-drain electrodes, which were prepared by photolithography. The gate dielectric layer has a capacitance of  $\approx 11.5 \text{ nF cm}^{-2}$ . The substrates were first subjected to cleaning by ultrasonication in acetone, deionized water, and ethanol. Next, OTS modification was performed in solution (hexane: OTS = 100:1) to form an OTS self-assembled monolayer on the surface of the dielectric. After removing the extra OTS by hexane, polymer semiconductor was deposited by spin coating from a preheated polymer solution in *o*-dichlorobenzene (10 mg mL<sup>-1</sup>) in N<sub>2</sub> glovebox. The samples were further annealed on a hotplate at 180 °C in N<sub>2</sub> for 10 min. BGBC FETs were measured in N<sub>2</sub> by using a Keithley 4200 SCS semiconductor parameter analyzer. Channel length ( $L$ ) and width ( $W$ ) of the devices were 20 and 1400  $\mu\text{m}$ , respectively.

**Reliability Factor Calculations:** Reliability factors of saturated mobility ( $r_{\text{sat}}$ ) for the polymers are calculated according to Equation (2)<sup>[27]</sup>

$$r_{\text{sat}} = \frac{\left( \frac{\sqrt{|I_{\text{DS}}^{\text{max}}|} - \sqrt{|I_{\text{DS}}^{\text{off}}|}}{|V_G|^{\text{max}} - |V_G|^{\text{off}}} \right)^2}{\left( \frac{\partial \sqrt{|I_{\text{DS}}|}}{\partial V_G} \right)} \quad (2)$$

where  $I_{\text{DS}}^{\text{off}}$  is minimum current at the off-state.

**Theoretical Calculations:** For simplicity, the alkyl chains at the thiophenes were replaced by methyl groups. The geometry structures of isolated polymer chain with 1D periodicity were optimized at HSE06-D3 functional with the CRYSTAL17 Package.<sup>[42]</sup> Uniform  $5 \times 1 \times 1$  Monkhorst–Pack  $k$ -point mesh was employed for all the polymers. To generate the band structures, 50  $k$ -points were calculated between the gamma point (center of the Brillouin zone (BZ)) and the edge of the first BZ.  $m^*$  for 1D crystal was calculated by means of Sperling's centered difference method with  $dk = 0.01 \text{ Bohr}^{-1}$  using the following definition

$$m^* = \hbar^2 / (d^2E/dk^2) \quad (3)$$

where  $E$  is the band energy and  $k$  is the electron wave vector along the backbone direction.

The mobility can be evaluated according to Equation (4)

$$\mu = e\tau/m^* \quad (4)$$

where  $e$  is the electron charge and  $\tau$  is the effective scattering time.  $\tau$  is limited by energetic disorder, dynamic disorder, and chain ends.<sup>[43]</sup> According to this equation, smaller  $m^*$  suggests better intramolecular charge transport along the polymer backbone, which is favorable to obtain high mobility.

## Supporting Information

Supporting Information is available from the Wiley Online Library or from the author.

## Acknowledgements

J.Y. and Y.J. contributed equally to this work. This work was financially supported by the National Natural Science Foundation of China (Grant No.s: 61890940, 51873216, 21504026, and 21633012), the National Key R&D Program of "Strategic Advanced Electronic Materials" (No. 2016YFB0401100), and the Strategic Priority Research Program of the Chinese Academy of Sciences (No. XDB12030100 and XDB30000000) and Key Research Program of Frontier Sciences, CAS, Grant No. QYZDY-SSW-SLH029 and Beijing Nova program (Z181100006218034). 2D-GIXRD results were obtained at 1W1A Station of Beijing Synchrotron Radiation Facility. The authors gratefully acknowledge the assistance of scientists of the Diffuse X-ray Scattering Station during the experiments.

## Conflict of Interest

The authors declare no conflict of interest.

## Keywords

ambipolar transistors, bay-annulated indigo, electron-withdrawing group substituted, high performance

Received: July 15, 2018  
Revised: November 25, 2018  
Published online:

- [1] L. Lu, T. Zheng, Q. Wu, A. M. Schneider, D. Zhao, L. Yu, *Chem. Rev.* **2015**, *115*, 12666.  
[2] A. C. Arias, J. D. MacKenzie, I. McCulloch, J. Rivnay, A. Salleo, *Chem. Rev.* **2010**, *110*, 3.

- [3] X. Guo, A. Facchetti, T. J. Marks, *Chem. Rev.* **2014**, *114*, 8943.  
[4] Z. Yi, S. Wang, Y. Liu, *Adv. Mater.* **2015**, *27*, 3589.  
[5] Z. Liu, G. Zhang, D. Zhang, *Acc. Chem. Res.* **2018**, *51*, 1422.  
[6] T. Lei, J.-Y. Wang, J. Pei, *Acc. Chem. Res.* **2014**, *47*, 1117.  
[7] K.-H. Ong, S.-L. Lim, H.-S. Tan, H.-K. Wong, J. Li, Z. Ma, L. C. H. Moh, S.-H. Lim, J. C. de Mello, Z.-K. Chen, *Adv. Mater.* **2011**, *23*, 1409.  
[8] Y. Zhao, Y. Guo, Y. Liu, *Adv. Mater.* **2013**, *25*, 5372.  
[9] J. Yang, Z. Zhao, S. Wang, Y. Guo, Y. Liu, *Chem* **2018**, *4*, 2748.  
[10] J. Zaumseil, R. H. Friend, H. Sirringhaus, *Nat. Mater.* **2006**, *5*, 69.  
[11] T. Bura, S. Beaupré, O. A. Ibraikulov, M.-A. Légaré, J. Quinn, P. Lévêque, T. Heiser, Y. Li, N. Leclerc, M. Leclerc, *Macromolecules* **2017**, *50*, 7080.  
[12] T. Lei, J.-H. Dou, Z.-J. Ma, C.-H. Yao, C.-J. Liu, J.-Y. Wang, J. Pei, *J. Am. Chem. Soc.* **2012**, *134*, 20025.  
[13] T. Lei, J.-H. Dou, Z.-J. Ma, C.-J. Liu, J.-Y. Wang, J. Pei, *Chem. Sci.* **2013**, *4*, 2447.  
[14] R. Schmidt, J. H. Oh, Y.-S. Sun, M. Deppisch, A.-M. Krause, K. Radacki, H. Braunschweig, M. Könemann, P. Erk, Z. Bao, F. Würthner, *J. Am. Chem. Soc.* **2009**, *131*, 6215.  
[15] G. Engi, *Z. Angew. Chem.* **1914**, *27*, 144.  
[16] B. He, A. B. Pun, D. Zherebetsky, Y. Liu, F. Liu, L. M. Klivansky, A. M. McGough, B. A. Zhang, K. Lo, T. P. Russell, L. Wang, Y. Liu, *J. Am. Chem. Soc.* **2014**, *136*, 15093.  
[17] K. J. Fallon, N. Wijeyasinghe, N. Yaacobi-Gross, R. S. Ashraf, D. M. E. Freeman, R. G. Palgrave, M. Al-Hashimi, T. J. Marks, I. McCulloch, T. D. Anthopoulos, H. Bronstein, *Macromolecules* **2015**, *48*, 5148.  
[18] K. J. Fallon, N. Wijeyasinghe, E. F. Manley, S. D. Dimitrov, S. A. Yousaf, R. S. Ashraf, W. Duffy, A. A. Y. Guilbert, D. M. E. Freeman, M. Al-Hashimi, J. Nelson, J. R. Durrant, L. X. Chen, I. McCulloch, T. J. Marks, T. M. Clarke, T. D. Anthopoulos, H. Bronstein, *Chem. Mater.* **2016**, *28*, 8366.  
[19] K. J. Fallon, A. Santala, N. Wijeyasinghe, E. F. Manley, N. Goodeal, A. Leventis, D. M. E. Freeman, M. Al-Hashimi, L. X. Chen, T. J. Marks, T. D. Anthopoulos, H. Bronstein, *Adv. Funct. Mater.* **2017**, *27*, 1704069.  
[20] M. A. Kolczkowski, B. He, Y. Liu, *Org. Lett.* **2016**, *18*, 5224.  
[21] J. Brebels, K. C. C. W. S. Klider, M. Kelchtermans, P. Verstappen, M. Van Landeghem, S. Van Doorslaer, E. Goovaerts, J. R. Garcia, J. Manca, L. Lutsen, D. Vanderzande, W. Maes, *Org. Electron.* **2017**, *50*, 264.  
[22] B. He, W. T. Neo, T. L. Chen, L. M. Klivansky, H. Wang, T. Tan, S. J. Teat, J. Xu, Y. Liu, *ACS Sustainable Chem. Eng.* **2016**, *4*, 2797.  
[23] B. He, D. Zherebetsky, H. Wang, M. A. Kolczkowski, L. M. Klivansky, T. Tan, L. Wang, Y. Liu, *Chem. Sci.* **2016**, *7*, 3857.  
[24] H. Li, F. S. Kim, G. Ren, S. A. Jenekhe, *J. Am. Chem. Soc.* **2013**, *135*, 14920.  
[25] R. S. Ashraf, I. Meager, M. Nikolka, M. Kirkus, M. Planells, B. C. Schroeder, S. Holliday, M. Hurhangee, C. B. Nielsen, H. Sirringhaus, I. McCulloch, *J. Am. Chem. Soc.* **2015**, *137*, 1314.  
[26] H. Chen, Z. Liu, Z. Zhao, L. Zheng, S. Tan, Z. Yin, C. Zhu, Y. Liu, *ACS Appl. Mater. Interfaces* **2016**, *8*, 33051.  
[27] H. H. Choi, K. Cho, C. D. Frisbie, H. Sirringhaus, V. Podzorov, *Nat. Mater.* **2017**, *17*, 2.  
[28] Y. Zhou, C. Fuentes-Hernandez, J. Shim, J. Meyer, A. J. Giordano, H. Li, P. Winget, T. Papadopoulos, H. Cheun, J. Kim, M. Fenoll, A. Dindar, W. Haske, E. Najafabadi, T. M. Khan, H. Sojoudi, S. Barlow, S. Graham, J.-L. Brédas, S. R. Marder, A. Kahn, B. Kippelen, *Science* **2012**, *336*, 327.  
[29] J. Yang, H. Wang, J. Chen, J. Huang, Y. Jiang, J. Zhang, L. Shi, Y. Sun, Z. Wei, G. Yu, Y. Guo, S. Wang, Y. Liu, *Adv. Mater.* **2017**, *29*, 1606162.

- [30] Y. Gao, Y. Deng, H. Tian, J. Zhang, D. Yan, Y. Geng, F. Wang, *Adv. Mater.* **2017**, *29*, 1606217.
- [31] B. Sun, W. Hong, Z. Yan, H. Aziz, Y. Li, *Adv. Mater.* **2014**, *26*, 2636.
- [32] B. Kang, R. Kim, S. B. Lee, S.-K. Kwon, Y.-H. Kim, K. Cho, *J. Am. Chem. Soc.* **2016**, *138*, 3679.
- [33] A. J. Kronemeijer, E. Gili, M. Shahid, J. Rivnay, A. Salleo, M. Heeney, H. Sirringhaus, *Adv. Mater.* **2012**, *24*, 1558.
- [34] J. Yang, Z. Zhao, H. Geng, C. Cheng, J. Chen, Y. Sun, L. Shi, Y. Yi, Z. Shuai, Y. Guo, S. Wang, Y. Liu, *Adv. Mater.* **2017**, *29*, 1702115.
- [35] H. Chen, Y. Guo, Z. Mao, G. Yu, J. Huang, Y. Zhao, Y. Liu, *Chem. Mater.* **2013**, *25*, 3589.
- [36] Z. Yan, B. Sun, Y. Li, *Chem. Commun.* **2013**, *49*, 3790.
- [37] T. Lei, J.-H. Dou, X.-Y. Cao, J.-Y. Wang, J. Pei, *Adv. Mater.* **2013**, *25*, 6589.
- [38] H. Wang, P. Chao, H. Chen, Z. Mu, W. Chen, F. He, *ACS Energy Lett.* **2017**, *2*, 1971.
- [39] Z. Hu, H. Chen, J. Qu, X. Zhong, P. Chao, M. Xie, W. Lu, A. Liu, L. Tian, Y.-A. Su, W. Chen, F. He, *ACS Energy Lett.* **2017**, *2*, 753.
- [40] M. Chu, J.-X. Fan, S. Yang, D. Liu, C. F. Ng, H. Dong, A.-M. Ren, Q. Miao, *Adv. Mater.* **2018**, *30*, 1803467.
- [41] Z. Mao, Y. Guo, H. Chen, W. Zhang, G. Yu, *Polymer* **2016**, *99*, 496.
- [42] A. Erba, J. Baima, I. Bush, R. Orlando, R. Dovesi, *J. Chem. Theory Comput.* **2017**, *13*, 5019.
- [43] B. B.-Y. Hsu, C.-M. Cheng, C. Luo, S. N. Patel, C. Zhong, H. Sun, J. Sherman, B. H. Lee, L. Ying, M. Wang, G. Bazan, M. Chabinyc, J.-L. Brédas, A. Heeger, *Adv. Mater.* **2015**, *27*, 7759.